PROSPECTS OF A HYBRID MAGNETIC/ELECTROSTATIC SAMPLE CONTAINER RETRIEVER

Takuma Shibata [*] **, Trevor Bennett,**[†] **and Hanspeter Schaub**[‡]

Space agencies and companies are evaluating possibilities for a Martian sample return mission for improving our understanding of planetary bodies within our solar system. However, the rendezvous docking in deep space requires automatic navigation and control because it is difficult to communicate with the explorer in real time. Perspective of a sample container retriever utilizing electro-static force and flux pinning force is discussed in this paper. The proposed method uses this electrostatic interaction to catch the Mars 2020 launched orbit sample container (OS) on orbit. The sample return container has three permanent magnets and the shape is designed as column to make the weight smaller and get Martian samples effectively. The proposed retriever must control angular velocity and attitude of the OS using electrostatic force to fetch. After controlling the OS, it is tugged to the orbiter and restrained safely using flux pinning effect. The feasibility of the proposed retrieval system is discussed from the aspect of the required energy and Debye length requirements. The controller is designed using a Lyapunov function and Mukherjee & Chen's theorem and the performance is discussed in this paper.

INTRODUCTION

Returning a sample from a planet provides the opportunity for various insights related to the formation and configuration of the planet. HAYABUSA succeeded in bringing particles from the asteroid Itokawa and now space agencies and space companies are looking at Martian sample return mission[1–5]. Unlike the HAYABUSA mission, an explorer can not take a sample using the touch-down method from a planet such as Mars because of the large fuel requirements to escape the planetary gravity. It has been proposed that an orbit sample container (OS) is launched using a Mars Ascent Vehicle (MAV) after Martian samples are collected by the Mars 2020 rover[6–8]. After launching the OS to an orbit, a Martian Sample Return (MSR) orbiter takes it back to the Earth and jettisons the OS protected by an Earth re-entry capsule[9–11]. However the MSR rendezvous with the OS is a challenging and unsolved aspect of the current mission architecture. An automatic catching system is desired for docking with the OS because time lag inhibits real-time communications between a ground station on the Earth and the orbiter[6]. To liberalize this difficulty of the control for the docking, there are ideas to retrieve the OS safely. The MSR orbiter has a camera used to detect the OS at a distance of $10,000$ km. The OS has an UHF beacon to help to inform the MSR with an alternate relative range measurement[3, 6].

---

[*]Graduate student, Department of Space and Astronautical Science, The Graduate University for Advanced Studies SOK-ENDAI, 3-1-1, Yoshinodai, Chuo-ku, Sagamihara, Kanagawa 252-5210, Japan .

[†]Graduate student, Aerospace Engineering Sciences, University of Colorado, 431 UCB, ECNT 320, Boulder, CO 80309-0431, USA.

[‡]Professor, Aerospace Engineering Sciences, University of Colorado, 431 UCB, ECNT 320, Boulder, CO 80309-0431, USA.
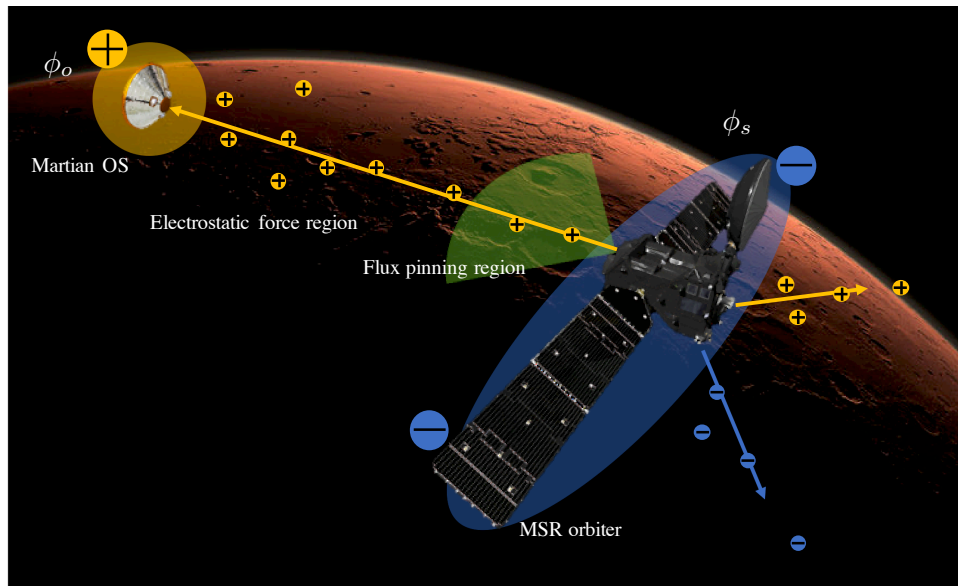
Figure 1. Hybrid Magnetic/Electrostatic Sample Container Retriever (Courtesy of ESA for the explorer and sample container photo and NASA for background photo)

A method using a mechanical arm has been considered as one of the ideas to restrain the OS on Martian orbit[12, 13]. This system mainly consists of a capture cone and lid. The capture cone lid starts to close when the OS enters in the capture cone with the relative position controlled by the orbiter. There is another plan to use the flux pinning effect for catching the OS[14]. The flux pinned container that might be used in Mars 2020 mission is designed in spherical shape. Its radius is approximately 0.17 m and it has multiple permanent magnets that allow the orbiter to catch the container with any attitude using the flux pinning effect[3, 5, 14]. However, cylinder shape is more useful because it provides better packing for cylindrical samples. In addition, this shape of the OS provides a benefit to the MAV. The cylindrical shape is useful rather than the spherical shape because the OS allows a smaller ascent vehicle diameter for the same lifted volume or mass. If a cylinder OS is used for the sample return mission, the attitude and angular velocity of the OS must be controlled for catching the OS safely. On-orbit debris capture is an area of research that may provide additional methods and approaches to the on-orbit capture of the OS.

The Magnetic Capture Device has been researched to automatically retrieve the OS[15]. A magnetorquer and permanent magnet are mounted on the orbiter. The OS has also a permanent magnet on the capture axis. The attitude and angular velocity are controlled by the magnetorquer on the orbiter. To solve the problem of space debris and collision of an asteroid to the Earth, the methods to control the state of a target have been researched using laser ablation and the coulomb force. Approaching to space debris may cause a dangerous situation as the space debris is rotating. Thus, control methods without direct contact have been investigated. Laser ablation technique has been considered as one of the methods to suspend the spinning rate of a space debris[16, 17] and an asteroid approaching to the Earth[18] as well. However, the laser ablation is not applicable for the sample container retriever because of destruction to the OS. In addition, the coulomb force has been considered to control spin rate of space debris[19–21].

A satellite on an orbit is charged up by electron and proton in plasma environment and those particles can be emitted from the satellite using an electron gun and an ion gun. The potential of the

satellite and target can be changed by emitting electron or ion. The potential difference between the target and the satellite enable to control the state of the target. The attitude of the satellite also is changed by action-reaction law but is maintained by reaction wheels and thrusters on the satellite. It is mentioned that the coulomb force can detumble the spin rate of a space debris whose size is huge compared with the operating orbiter[20,21]. An experiment was performed to confirm if the coulomb interaction is useful for controlling the spinning rate of a space debris and the results showed this method is useful for detumbling[22–24].

The proposed system consists of a cylindrical OS and the detumbling method using the coulomb force as Fig.1. The advantage of using coulomb force is that the OS does not need any actuator. Simple system is desired for the automatic rendezvous docking phase. In addition, the container is experienced twice launching and once entry in Mars, therefore complicated system is not favorable. The OS does not require dozens of permanent magnets because the attitude is controlled by the orbiter, hence the mass of the OS can be decreased. Furthermore this retrieval system using the coulomb force can control the attitude and spinning rate of the OS while tugging.

It is assumed that the OS is launched by a small rocket and then a Martian orbiter fetches the OS using the proposed system on an orbit at 600 km. The orbiter controls the state of the OS to be desired state with 6 degrees of freedom (DOF). As a problem, the operation for detumbling and rendezvous docking on Martian orbit at 600 km must be conducted with limitation resource because of plasma characteristic, which is dense and low energy compared with orbital debris studies conducting in Earth Geosynchronous Orbit (GEO). The achievable altitude of an orbit depends on the performance of the launcher and it is difficult to send the OS to high altitude orbit such as GEO. To use the coulomb force detumbling method on this orbit requires an ion/electron gun to operate with high energy if the orbiter needs high potential to control the target's state.

The goal of this paper is to explore the feasibility and benefits of the proposed system in terms of the power, Debye length, and control system. The performance of the proposed system is discussed under those limitations. This paper consists of six sections. The second section mentions about the required power to operate this system and the Debye length which are fundamental parameters for operating the electrostatic force in plasma environment . Required power determines the maximum potential that the orbiter can use to control the state of the OS. The proposed retrieval system must be operated in the range of the Debye length because the electrostatic field (E-field) is screened beyond the range. The third section mentions force distribution between the OS and the orbiter. This proposed retrieval system utilizes the coulomb force to control the attitude and angular velocity and flux pinning force which is used to catch the OS automatically in close distance. Lorentz force affects on the OS and the orbiter because of permanent magnets on the OS. The relationship of those forces depending on the relative distance is shown in this section. Nonlinear controller design is shown in the forth section. Lyapunov function is applied to design the controller for the attitude and angular velocity of the OS. Those results of the controller performance is shown in the fifth section.

HYBRID MAGNETIC/ELECTROSTATIC SAMPLE CONTAINER RETRIEVER

The MSR orbiter has two electron guns and an ion gun to control the potential of itself and the orbital sample (OS) target. The potential of the OS is controlled to be constant by getting an ion from the ion gun on the orbiter. Another ion gun and the electron gun on the orbiter operate to change the potential of itself. In addition, the orbiter has type-II superconductors and electromagnetic coils because the flux pinning effect is used for automatic catching system utilizing flux
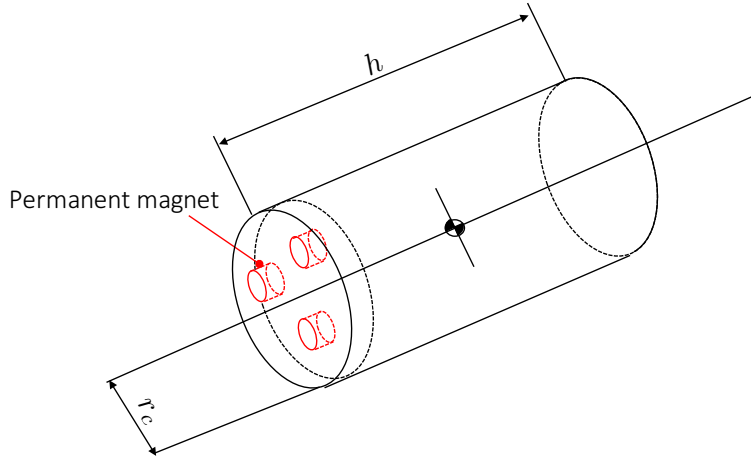
Figure 2. Cylindrical sample container configuration

pinning interface (FPI)[25] in the docking phase. The shape of the OS is designed as column and it has three permanent magnets on bottom of one side in this study as Fig.2. The cylindrical OS allows to collect a Martian sample effectively compared with the spherical sample canister because every Martian sample, which are stratum, sand and rocks, are stowed into a cylinder capsule after the Martian sample is collected by the Mars Exploration Rover (MER). Besides the weight of this OS can be reduced because only three permanent magnets are mounted. For these reasons, it is assumed that the cylindrical OS is used for a sample return mission in this paper. This OS has three permanent magnets on the bottom of one side to benefit the flux pinning effect in the docking phase. If the OS is used for the MSR mission, however, the angular velocity and attitude of the OS must be controlled to catch safely using the flux pinning effect. As a control method for the OS, the coulomb force is used. The control method using coulomb force allows the orbiter to control the state of the OS which does not need to have any actuators to control the state of itself. The OS is tugged into the range of the flux pinning effect while controlling the attitude and angular velocity using the coulomb force. Finally, the rendezvous docking using the FPI operates when the OS enter into the range of the flux pinning effect. In this section, the fundamental information required to use the electrostatic control system is given and the limited conditions are shown on the Martian orbit.

Debye shielding on the Martian low orbit

When the electrostatic interaction works in plasma environment, the Debye shielding effect occurs. If the interaction between charged particles is considered in vacuum environment, the coulomb force, related to Laplace potential field, is not interrupted by the Debye shielding effect[26–28]. However, the Debye length should be cared for the electrostatic interaction between infinite charged bodies[29–33]. The Debye length is important parameter because the E-field rapidly decreases beyond this length by the Debye shielding effect. The E-field $E(\boldsymbol{r})$ of a charged body A, which potential is V_A, can be expressed as following in plasma environment using the electron Debye length λ_D:

$$E(\boldsymbol{r}) = -\nabla_r \phi(\boldsymbol{r}) = \frac{V_A R_A}{r^2} e^{-(\boldsymbol{r}-\boldsymbol{R_A})/\lambda_D}(1 + \frac{\boldsymbol{r}}{\lambda_D}). \qquad (1)$$

where $\boldsymbol{r}$ and $\boldsymbol{R_A}$ are the distance from the charged body A and the radius respectively. This expression shows that the E-field decreases exponentially as the distance from the body A becomes bigger

4

Table 1. Parameters in plasma on Martian orbit at 600 km

Particle	Density [$1/cm^3$]	Temperature [eV]
Ion	50	0.63
Electron	20	0.42
Photon	-	0.4

than the electron Debye length. The electron Debye length can be expressed as

$$\lambda_D = \sqrt{\frac{\epsilon_0 T_e}{n_e q_e^2}} \qquad (2)$$

where ϵ_0 is the permittivity of vacuum and q_e [C] is electron charge. This electron Debye length is depending on the density n_e [$1/cm^3$] and temperature of the electron T_e [eV]. This length becomes longer on orbit with high altitude[34, 35] because the density becomes smaller although the temperature becomes also denser. Therefore it has been considered that detumbling method and formation flying using the coulomb force are used on GEO[20, 21, 29, 36, 37].

However the electron Debye length cares only the electron physics although electron and ion are mixing neutrally in plasma. This means the expression cares only the case of the plasma physics in timescales which is longer than the motion of ions[38]. For this assumption, the electron Debye length is not useful to estimate the range of the coulomb force for this system. Moreover this electron Debye length can not take account of the interaction between finite bodies. The Debye shielding effect can be accounted using Debye Hückel model more accurately. Effective Debye length $\bar{\lambda}_D$ is proposed to solve the range of the coulomb force for finite charged bodies[39]. The effective Debye length $\bar{\lambda}_D$ assumes that the electron Debye length λ_D is related lineally to the effective Debye length using the scaling factor σ as

$$\bar{\lambda}_D = \sigma \lambda. \qquad (3)$$

This effective Debye length is more accurate than the electron Debye length and can account the effect of the size and potential of a charged body in unperturbed plasma environment. Hence this effective Debye length model is applied for the proposed sample container retrieval system.

It is assumed the Martian OS is launched on the orbit at 600 km. The plasma characteristics are dense and low energy on this orbit compared with high altitude orbit as GEO. This characteristics make the Debye length shorter distance. The orbiter is approximated as sphere, whose the radius changes from 0.5 to 4.0 m. The potential of the orbiter is changed from 5 to 55 kV in this calculation and the dependance are shown in this section. The value of the plasma parameters are referred to the data observed by the Viking I, MAVEN and MARSIS[40–45]. Those parameters are shown in Table.1 and used in this paper. The σ is solved as Fig.3 using those parameters. As seen in the Fig.3, the green surface is the scaling factor σ on the Martian orbit at 600 km. This scaling factor is intricately depending on not only the parameter of the orbiter but also the characteristics of plasma and currents generated on the orbiter. Regression analysis is conducted to get easy way to calculate the effective Debye length using the result of Fig.3[26]. The scaling factor σ depending on the radius R_A and potential ϕ of the orbiter is expressed as

$$\sigma(\phi, R_A) = (1 + \phi)f(\phi, R_A) + (1 + R_A)\log\phi \qquad (4)$$

where $f(\phi, R_A)$ is given as the first order polynominal function. The scaling factor σ is derived as
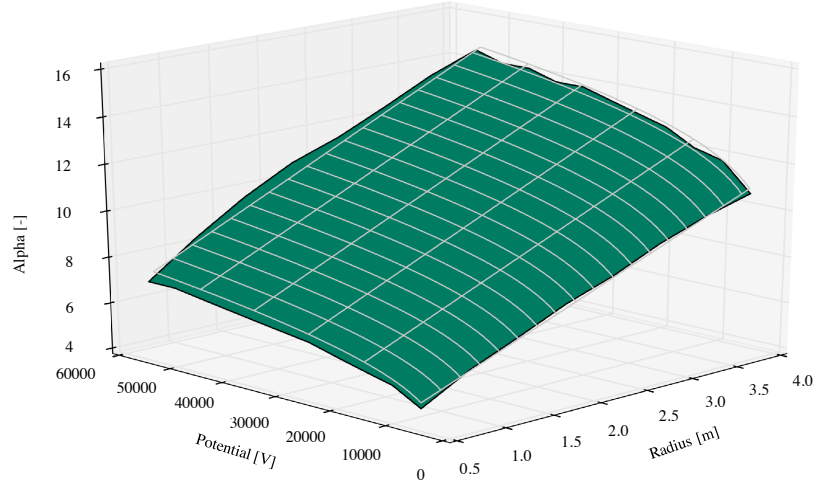
Figure 3. Alpha depending on the potential and radius of the orbiter approximated as sphere

following expression to fit numerically computed scaling factor σ:

$$\sigma = -2.6221 + 1.758 \times 10^{-5}\phi - 5.28 \times 10^{-11}\phi^2$$
$$-1.73 \times 10^{-7}R\phi + 0.4296R + 0.7826\log\phi + 0.1434R\log\phi. \quad (5)$$

This Eq.5 is given by multilinear regression model. When the effective Debye length is estimated on the target orbit for this proposed system, this σ using Eq.5 has tremendous advantage because the scaling factor σ allows to easily calculate the effective Debye length. This regression expression is shown in Fig.3 as white line and is evaluated as the coefficient of determination $R^2 = 0.991$. The dependance on the size and potential of the orbiter is expressed as Fig.4 using the regression expression. The bigger the radius and potential of the orbiter is, the larger the effective Debye length is. Although the size of the orbiter is limited by the fairing of a rocket, the effective Debye length becomes over 10m if the explorer size is allowed by the rocket's fairing. However, the effective Debye length is still short distance compared with GEO's Debye length which is over 100m even if the potential and the size becomes bigger because of the orbit.

Power requirement to operate the proposed retriever

Ions and electrons must be emitted with enough of power to leave from the E-field of the MSR orbiter because those particles can come back. The orbiter in this study has two ion guns and an electron gun to change the potential of the Martian OS and the orbiter. One of the ion guns is directed to the Martian OS to shoot ions. The other ion gun and electron gun are used to control the potential of the orbiter. The orbiter is charged up by several factors in plasma environment[34,35]. Currents caused by several factors flow on the OS and the orbiter as well and those factors are divided into the way to charge of a body in plasma, which is divided by primary charging process and secondary emission. The primary charging process is caused by not only plasma environment but also photoelectron from the solar activity. Electrons, ions and photoelectrons come into the body in plasma and those action causes for generating currents on the body. In addition to the primary charging process, secondary electron emission occurs when ions are absorbed by the OS.
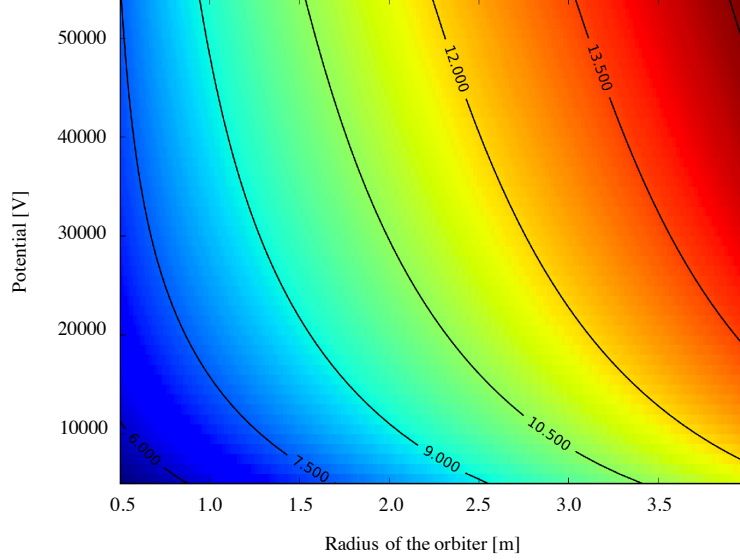
Figure 4. Effective Debye length depending on the potential and radius of the orbiter approximated as sphere

This secondary emission occurs when the primary ion, which is shot from the ion gun on the orbiter, is impacted into the potential barrier of the OS. Then secondary electrons are emitted by the primary emission. It is assumed that the potential of the OS is maintained to be constant and the potential of the orbiter is only controlled. Those currents generated by the impact of those particles can be expressed numerically. Those expressions are shown and required power to operate the proposed retrieval system is estimated in this section.

Photoelectron current is generated on a body A which receives energy of sun light. This photoelectron current can be expressed as

$$
\begin{aligned}
I_{ph}(\phi_A) &= j_{ph,0} A_\perp e^{-\phi_A/T_{ph}} & \phi_A > 0 \\
&= j_{ph,0} A_\perp & \phi_A \leq 0
\end{aligned}
\tag{6}
$$

where ϕ_A is the potential of the body A, T_{ph} is the temperature of the photoelectrons, and $A_\perp = \pi r_o^2$, which r_o is radius of the sphere as the orbiter, is the cross sectional area exposed to solar radiation. $j_{ph,0}$ is the photoelectron current and depending on the distance from the sun as[46]

$$
j_{ph,0} = j'_{ph,0} \left(\frac{r_e}{r_m} \right)^2
\tag{7}
$$

where $r_m = 1.5$ AU is the distance between Mars and Sun, $r_e = 1.0$ AU is the distance between the Earth and Sun and $j'_{ph,0}$ is the photoelectron current on a orbit around the Earth. As photoelectron current on the orbit around the Earth is assumed as $20\mu A/m^2$[35,47], the current on the Martian orbit is derived as $8.9\mu A/m^2$. From this result, the photoelectron current is defined as $10\mu A/m^2$ in this paper.

Electron current is modeled as[48]

$$I_e(\phi_A) = -\frac{Aqn_e\omega_e}{4}e^{\phi_A/T_e} \qquad \phi_A < 0$$
$$= -\frac{Aq_en_e\omega_e}{4}\left(1 + \frac{\phi_A}{T_e}\right) \qquad \phi_A \geq 0 \tag{8}$$

where $A = 4\pi r_o^3$ is the surface area of the orbiter, q is the elementary charge, n_e is the density of electrons and $\omega_e = \sqrt{8T_e/\pi m_e}$ is the thermal velocity of electrons. Mass of electron is $m_e = 9.11 \times 10^{-31}$ kg.

Ion current is modeled as[48]

$$I_i(\phi_A) = \frac{Aqn_i\omega_i}{4}e^{\phi_A/T_i} \qquad \phi_A > 0$$
$$= \frac{Aq_in_i\omega_i}{4}\left(1 - \frac{\phi_A}{T_i}\right) \qquad \phi_A \leq 0 \tag{9}$$

where n_i is the density of ions, $\omega_i = \sqrt{8T_i/\pi m_i}$ is the thermal velocity of ions. $m_i = 1.67 \times 10^{-27}$ kg and T_i are the mass and the temperature of ions respectively.

Electrons must be emitted from the orbiter with enough of energy to intrude in the potential barrier of the OS. When the OS receives electrons emitted by the electron gun on the orbiter, the electron current $I_{tr,2}$ flows. This electron current on the OS is depending on the energy of the electron gun E_{tr} and the both potential of the orbiter ϕ_o and OS ϕ_s. The current I_{tr2} is modeled as follow:

$$I_{tr2}(\phi_D) = -\delta I_{tr} \qquad q\phi_s - q\phi_o < E_{tr}$$
$$= 0 \qquad q\phi_s - q\phi_o \geq E_{tr} \tag{10}$$

where I_{tr} is the beam current operated by the orbiter. δ is the efficiency of the transfer and this coefficient is dealt as 1.0 in this paper. It is assumed that the parameter of the ion gun's energy is depending on the potential of the orbiter and can be expressed as the condition of the Eq.10.

Secondary effect current flows on the OS when it receives ions from the orbiter. This current can be calculated using following expression as[49]

$$I_{SEE}(\phi) = -4Y_M I_D(\phi_D)K \qquad \phi_A < 0 \ and \ I_{tr} > 0$$
$$= \frac{Aq_in_i\omega_i}{4}\left(1 - \frac{\phi}{T_i}\right) \qquad \phi_A \geq 0 \ or \ I_{tr} < 0, \tag{11}$$

where

$$K = \frac{E_{eff}/E_{max}}{(1 + E_{eff}/E_{max})^2}, \tag{12}$$

and

$$E_{eff} = E_{EB} - q(\phi_s - \phi_o). \tag{13}$$

Y_M is the maximum yield of secondary electron production and E_{max} is the maximum impact energy, which values are depending on a material,. In this study, it is assumed that aluminum is used for the material of the OS and then $Y_M = 2$ and $E_{max} = 300$ eV.

In this study, it is assumed that the potential of the OS is maintained by achieving the net current balance on the OS. The ion gun on the orbiter operates to make the potential of the OS to be positive

Table 2. The required total power to operate the hybrid sample container retriever

Particle	Transfer	External	Total power
$\phi_s = +10kV$ $\phi_o = -10kV$	$I_{tr} = 0.91$ mA $E_{tr} = 20$ keV $P_{tr} = 18.2$ W (i$^+$)	$I_{ex} = -5.89$ mA $E_{ex} = 10$ keV $P_{ex} = 58.9$ W (i$^+$)	77.1 W
$\phi_s = +10kV$ $\phi_o = +10kV$	$I_{tr} = 0.91$ mA $E_{tr} = 0$ keV $P_{tr} = 0$ W (i$^+$)	$I_{ex} = 102.9$ mA $E_{ex} = 10$ keV $P_{ex} = 1029$ W (e$^-$)	1029 W

and constant. For this assumption, the ion guns must operate to meet following conditions for the positive potential of the orbiter:

$$I_{e,s} + I_{tr2,s} = 0. \tag{14}$$

As the potential of the orbiter is positive, the ion current I_i, the photoelectron current I_{ph} and the secondary effect can be neglected. If the orbiter's potential becomes negative, then the currents balance expression is written as

$$I_{e,s} + I_{i,s} + I_{SEE,s} + I_{ph,s} + I_{tr2,s} = 0. \tag{15}$$

In addition, the ion and electron guns to control the potential of the orbiter also must operate under the following condition:

$$I_{ex} = -I_{tr} - I_{ph,o} - I_{e,o} - I_{i,o}. \tag{16}$$

The ion or electron gun must emits the current I_{ex} for controlling the potential of the orbiter. The power to transfer the ion and emit electrons and ions is function of the beam energy and transfer current of the ion gun on the orbiter:

$$P_{tr} = \frac{E_{tr}|I_{tr}|}{q_b}. \tag{17}$$

If the radius of the explorer becomes bigger, then the higher currents are generated by collision of those particles. This means the higher total operation power for the ion gun and electron gun is required to control the potential of the orbiter and the OS in plasma environment. In this paper, the radius of the orbiter is defined as 1.0 m, the maximum potential, which the orbiter can use, is ± 10 kV and the relative distance between the orbiter and the OS is 3.0 m which is in range of the effective Debye length. The shape of the OS is column shape as Fig.2 and the height h and radius r_c are defined as 0.3 m and 0.05 m respectively.

Then the current, required power is calculated as Tab.2. As seen in Tab.2, the maximum total power is estimated roughly 1029 W under the condition of the size and the maximum potential. The different polarity of those charged body is desirable because the attitude of the OS must be aligned to the orbiter. Therefore, it does not occur that the potential of the orbiter becomes the maximum and positive potential if the potential of the OS is positive potential. It is expected that the maximum power can be reduced when the potential of the orbiter and the OS are $+10$ kV. The property is discussed in the section about the control results in this paper.

FORCE DISTRIBUTION BETWEEN THE MSR ORBITER AND THE MARTIAN OS

The coulomb force and the flux pinning force are utilized to fetch automatically the Martian OS in the proposed method. The pinning force acts in close distance although the force is depending

on the parameters of a type-II superconductor (SC) and permanent magnet (PM). This force behaves repulsively before external magnetic flux intrudes into SC which is cooled below the critical temperature because of the Meissner effect. Once external magnetic flux is pinned in the SC, the force works as retentive force. This effect allows to maintain the relative state between the material generating magnetic flux, which is PM in this paper, and the cooled SC with more than 6 DOF passively. The coulomb force is used to control the relative states between the OS and the orbiter before catching the OS using the flux pinning effect. Lorentz force affects , however, because the OS has three PM and is approaching to the orbiter with velocity. This section shows the calculation model for those force to definitize the distribution of the forces in the effective Debye length between the Martian OS and the MSR orbiter.

Pinning force

Frozen image model is used to estimate the pinning force[50,51]. Two images, which are called frozen image and mobile image, are used to estimate easily the pinning force as Fig.5. Those images are generated when the SC is cooled below the critical temperature, which the temperature is depending on the kind of the SC. In the case of YBaCuO, the temperature is around 93 K. In other words, the pinning force is calculated using two images which are generated at equilibrium point in this numerical model. This pinning force works when the relative distance between the PM and the SC is changed. This model assumes that the pinning force is the sum of the magnetic force affecting between the pinned PM and the magnetic field generated by two images in the SC. M_p, M_f and M_m are the magnetic moment of the PM, frozen image and mobil image respectively. The relationship of those magnetic vectors is defined as $M_p = M_f = -M_m$ if only vertical motion of the PM is considered. The magnetic moment vector is expressed as $M_p = r_p^2 \pi h_p m_z$ where the radius r_p, height h_p and magnetization m_z of the PM. The magnetic force between the frozen image and the PM F_f is expressed as[14]

$$F_f = \mu_0 \nabla (H_f \cdot M_p) \tag{18}$$

where the magnetic field generated by the frozen image H_f is

$$H_f = \frac{1}{4\pi r_f^3} \left\{ -M_f + \frac{3(M_f \cdot r_f)}{r_f^2} r_f. \right\} \tag{19}$$

The position vector r_f and r_m between the PM and the images can be expressed as

$$r_f = r - r_{FC} + 2(a \cdot r_{FC})a, \tag{20}$$

$$r_m = 2(a \cdot r)a, \tag{21}$$

where r is the position vector between the PM and a point located on the surface of the SC, r_{FC} is the position vector between the PM at initial position and the point and a is the unit vertical vector on the surface. Finally, the pinning force F_p is expressed as the sum of the magnetic force between the PM and each image:

$$F_p = F_f + F_m. \tag{22}$$

If three permanent magnets are put on the bottom of the OS as vertexes of the equilateral triangle as Fig. 2, then the vertical pinning force can be written easily as[52]

$$F_{pz} = \frac{9\mu_0 M_z^2}{2\pi} \left[\frac{1}{\{2(z_i + z)\}^4} - \frac{1}{(2z_i + z)^4} \right]. \tag{23}$$

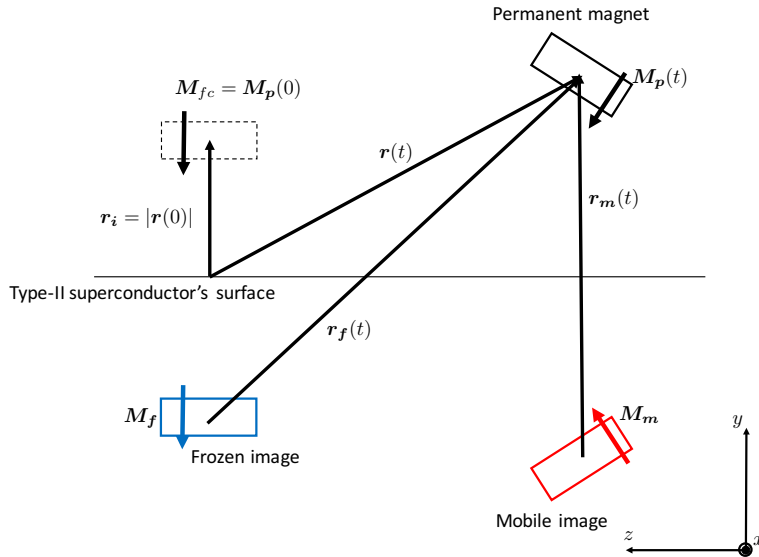This expression is used to estimate the pinning force affecting on the OS.

Figure 5. Frozen image model

Lorentz force

The lorentz force $\boldsymbol{F_{L,s}}$ works on the charged body by the external E-field $\boldsymbol{E_s}$ and the magnetic field $\boldsymbol{B_m}$ from PM on the Martian OS. The force affected on the OS behaves as

$$\boldsymbol{F_{L,s}} = -q_o \left\{ \boldsymbol{E_s} + \boldsymbol{v} \times \boldsymbol{B_m} \right\} \tag{24}$$

where q_o and $\boldsymbol{v}$ denote the charge of the orbiter and the relative velocity between the MSR orbiter and the OS. In this paper, first term $-q_o \boldsymbol{E_s}$ of Eq.24 is called as the coulomb force and second term $-q_o(\boldsymbol{v} \times \boldsymbol{B_m})$ is called as the magnetic force. Multi Sphere Model (MSM) is used for calculating the coulomb force affecting between the OS and the orbiter[19]. The coulomb force can be calculated using Finite Element Model(FEM). However, FEM takes time to estimate although FEM have high fidelity[23]. MSM model assumes the charged body as mass of spheres and calculates the electrostatic interaction between the charged bodies constructed by those spheres. In this calculation, the orbiter and the OS are assumed as one sphere and three spheres as Fig.6. The spheres constructing the OS are dubbed as sphere1, 2 and 3 in this paper. The potential of each sphere q_i is interacted with others and the interaction can be defined as following:

$$\phi_i = k_c \frac{q_i}{R_i} + \sum_{j=1,j\neq i}^{m} k_c \frac{q_j}{r_{i,j}} \tag{25}$$

where ϕ_i is the potential, k_c is Coulomb's constant, R_i is the radius of a sphere i, and $r_{i,j}$ is the distance between center of the sphere i and j. $r_{i,j}$ is defined as $\boldsymbol{r_{i,j}} = \boldsymbol{r_j} - \boldsymbol{r_i}$ where $\boldsymbol{r_i}$ and $\boldsymbol{r_j}$ are the position vector from the center of the total body, which consists of those spheres, to the sphere i and j respectively. Eq. (25) can be rewritten using Position Dependent Capacitance (PDC) C_M as

$$\phi = k_c \left[C_M \right]^{-1} \boldsymbol{q} \tag{26}$$
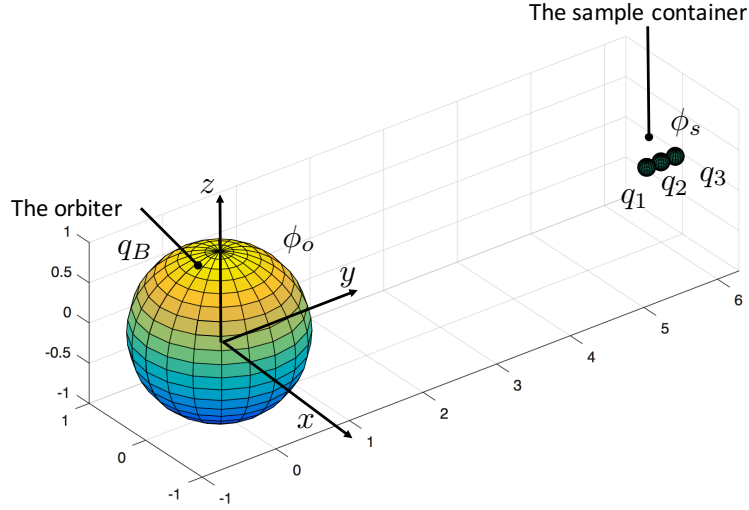
Figure 6. Multi Sphere Model for the proposed system

where

$$[C_M]^{-1} = \begin{bmatrix} 1/R_1 & 1/r_{1,2} & \dots & 1/r_{1,n} & 1/r_{1,B} \\ 1/r_{2,1} & 1/R_2 & \ddots & \vdots & \vdots \\ \vdots & \ddots & \ddots & \vdots & \vdots \\ 1/r_{n,1} & \dots & \dots & 1/R_n & 1/r_{n,B} \\ 1/r_{B,1} & \dots & \dots & 1/r_{B,n} & 1/r_B \end{bmatrix}. \tag{27}$$
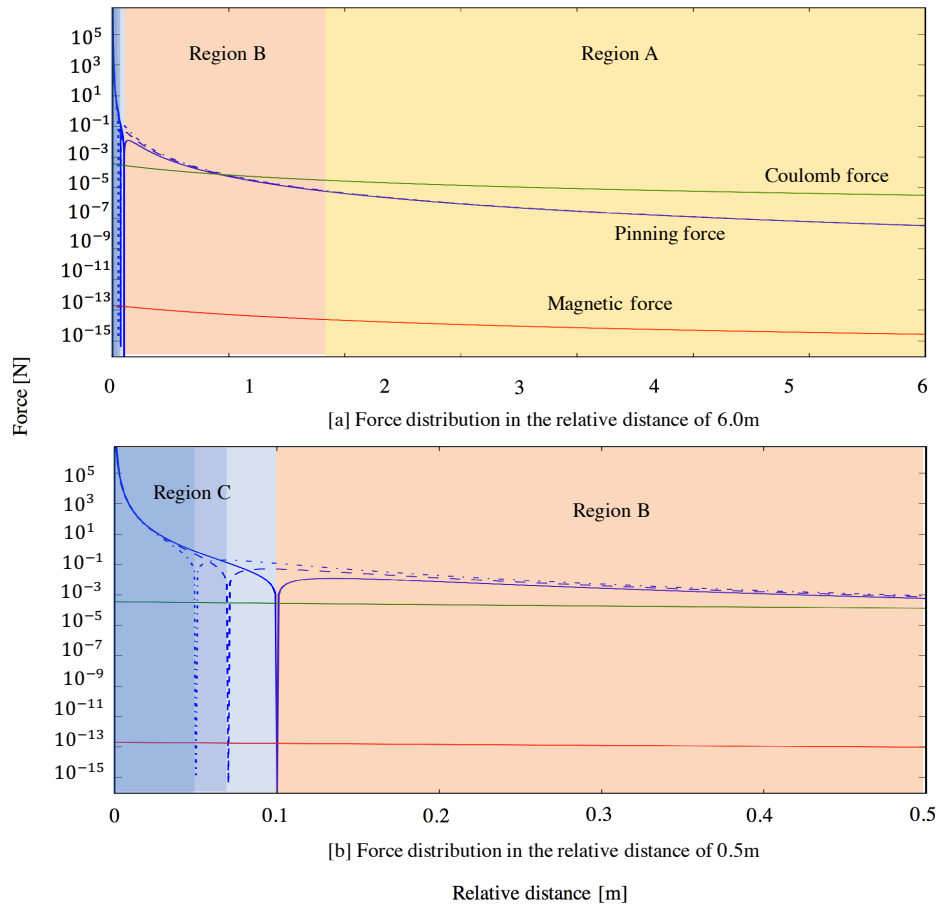
The charge of each sphere depending on the potential is given using Eq.(26). The coulomb force affecting between the OS and the orbiter can be expressed as

$$\boldsymbol{F_{c,s}} = k_c q_o \sum_{i=1}^{n} \frac{q_i}{r_{i,B}^3} \boldsymbol{r_{i,B}}. \tag{28}$$

Forces distribution

The relative velocity between the Martian OS and the MSR orbiter is assumed as $\boldsymbol{v} = [0, 0, 10]^t$ m/s for calculating the Lorentz force. The radius, height and magnetization of the PMs are 0.01 m, 0.01 m and 7.41×10^5 A/m respectively and three magnets are mounted on the OS. The result of the force distribution map between the OS and the obiter is shown as Fig.7. As seen in Fig.7, the pinning force becomes dominant in the region C and coulomb force becomes bigger than other forces in the region A. The magnetic force can be neglected although the force is affected between the orbiter and the OS in all of regions for simplicity. In region B, the coulomb force is smaller than the pinning force. This means the coulomb force can not control the OS from initial pinning point after the PMs on the OS is pinned in the SC. If it is required that the position of the OS is changed after pinned, the electron magnetic coil, which is mounted on the orbiter for the FPI docking system, must be operated.

The pinning force might become smaller than this result calculated by the frozen image model because the process to intrude the external magnetic flux into the cooled SC. There are two ways to

[a] Force distribution in the relative distance of 6.0m

[b] Force distribution in the relative distance of 0.5m

Relative distance [m]

Figure 7. Force distribution

generate the flux pinning effect, which are called as zero field cooling (ZFC) and field cooling (FC). FC is the way that a SC is cooled below the critical temperature while external magnetic flux is intruding in the SC. ZFC is the way that external magnetic flux is forcibly intruded into the SC. This frozen image model can estimate the FC pinning force rather than the ZFC pinning force. However, the magnetic flux generated by the PM is pinned in the cooled SC in the way of ZFC in this system. It is known that the FC pinning force becomes bigger than ZFC pinning force, therefore the region C might become smaller region than this result. The characteristics of the pinning force of ZFC and FC are not different so much, so this frozen image model was used for simplicity in this calculation. The coulomb force dominantly affects in the distance over 1.5 m in the region A of the Fig.7. To simplify the control the state of the OS, it is considered that the distance between the OS and the orbiter is fixed at 3.0 m which means that magnetic force and the pinning force can be neglected as the controller is activating.

NONLINEAR CONTROLLER DESIGN

Equation of motion for the sample container retriever

It can be said that only the coulomb force affects on the OS in yellow region of Fig.7 if the relative distance can be kept. It is assumed that the orbiter uses thrusters to maintain the relative distance for simplification. The coulomb force is used to control the attitude and angular velocity of the OS

13
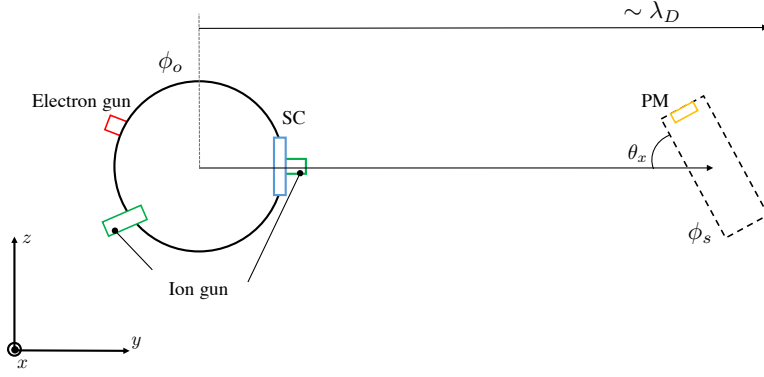
Figure 8. Retrieval system for fetching the Martian orbital sample container

in this paper. The torque to control can be expressed using MSM as

$$\boldsymbol{L_{cx}} = -k_c q_B \sum_{i=1}^{n} \frac{q_i}{r_{i,B}^3} \boldsymbol{r_i} \times \boldsymbol{r_{i,B}} \tag{29}$$

where $\boldsymbol{r_{i,B}}$ is $\boldsymbol{r_B} - \boldsymbol{r_i}$ and $\boldsymbol{r_B}$ is the position vector from a sphere of the OS to the orbiter. The torque with respect to x axis is calculated as Fig.9 using the expression. The simple torque is modeled by referring the result of the coulomb torque as

$$L_x = \gamma f(\phi) g(\theta_x) \tag{30}$$

where $f(\phi) = \phi$ is a function depending on the potential. $g(\theta_x) = \sin 2\theta_x$ expresses the dependance of the torque on the angle θ_x. γ is a scaling factor and depending on the sign of the potential as

$$\gamma(sign(\phi)) \begin{cases} \gamma_n & \phi < 0 \\ \gamma_p & \phi > 0 \end{cases} \tag{31}$$

This scaling factor γ is always positive, but the value is changed by the sign of the potential. Two dimensional rotation motion is considered in this paper, and then the motion of equation is given as

$$I_{xx} \ddot{\theta}_x = L_x \tag{32}$$

When it is considered that only the electrostatic interaction is affecting between the OS and the orbiter, the Euler's equation can be written as following expression by substituting the modeled coulomb torque:

$$I_{xx} \ddot{\theta}_x - \gamma f(\phi) g(\theta_x) = 0. \tag{33}$$

The controller is designed to converge the angular velocity and the attitude of the OS to be zero for this proposed system.

Stability analysis for the controller

In this section, the stability of the controller is discussed. The controller must make the state of the OS to be zero, which means $\theta_x \to 0$ and $\dot{\theta}_x \to 0$. The Lyapunov function is used for designing the controller and understanding the stability. The Lyapunov function candidate is designed as

$$V(\boldsymbol{\theta}) = \ln(1 + \sin^2 \theta_x) \frac{\gamma \phi_{\max}}{\beta} + \frac{1}{2} J_{xx} \dot{\theta}_x^2 \tag{34}$$

14
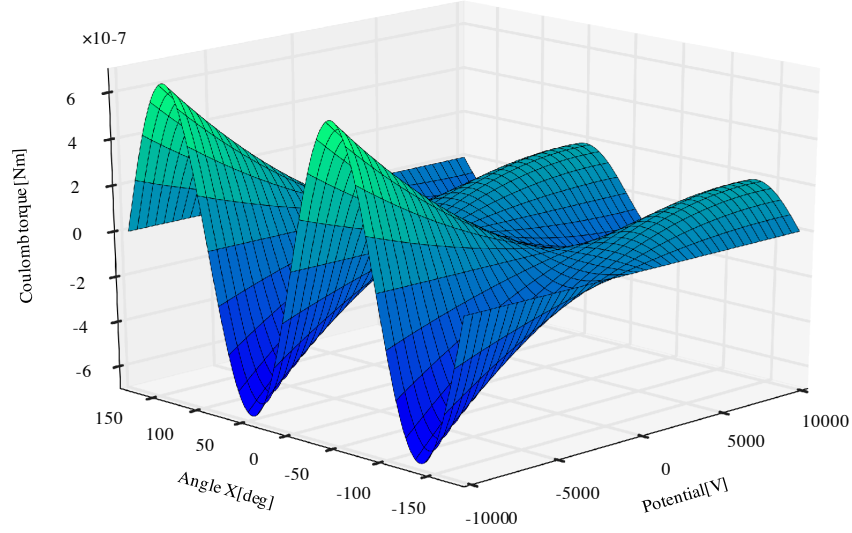
Figure 9. Coulomb torque calculated by Multi Sphere Model when the relative distance between the OS and the orbiter is 3.0 m

where $\boldsymbol{\theta} = (\theta_x, \dot{\theta}_x)$. This Lyapunov function $V(\boldsymbol{\theta})$ is 0 when $\boldsymbol{\theta} = 0$ and $V(\boldsymbol{\theta}) \geq 0$ for the range of ± 90 deg as seen in Fig.10. When the attitude of the OS is beyond this range of ± 90 deg, following sequence must be conducted:

$$
\begin{aligned}
\theta_x(t + dt) &= \theta_x(t) - 180 \quad \theta_x > 90 \\
\theta_x(t + dt) &= \theta_x(t) + 180 \quad \theta_x < -90
\end{aligned}
\tag{35}
$$

The first derivative Lyapunov function is given as

$$
\dot{V}(\boldsymbol{\theta}) = \gamma \left[\frac{\phi_{max}}{\beta(1 + \sin^2(\theta_x))} + f(\phi) \right] \dot{\theta}_x \sin(2\theta_x).
\tag{36}
$$

The Mukherjee and Chen's theorem (M&C's theorem) is used for the controller which allows the attitude and the angler velocity to be asymptotically stable. The first derivative Lyapunov function $\dot{V}(\boldsymbol{\theta})$ always should be negative definite or semi definite to make the system asymptotic stable according to the M&C's theorem. Then the controller for this retrieval system is designed as following to make the first derivative Lyapunov function $\dot{V}(\boldsymbol{\theta}) \leq 0$:

$$
\phi = -\frac{\phi_{max}}{\beta} \left(g(\theta_x) h(\alpha\dot{\theta}_x) + \frac{1}{1 + \sin^2(\theta_x)} \right)
\tag{37}
$$

where α and β are the gain for this controller and the scaling factor. h function is written as

$$
h(\alpha\dot{\theta}_x) = \frac{\tan^{-1}(\alpha\dot{\theta}_x)}{\pi/2}
\tag{38}
$$

Two subsets are defined as $Z_1 = \{\boldsymbol{\theta}|\theta_x = 0\}$ and $Z_2 = \{\boldsymbol{\theta}|\dot{\theta}_x = 0\}$ to analyze the stability of the controller using the M&C's theorem. When the second derivative Lyapunov function is considered

15
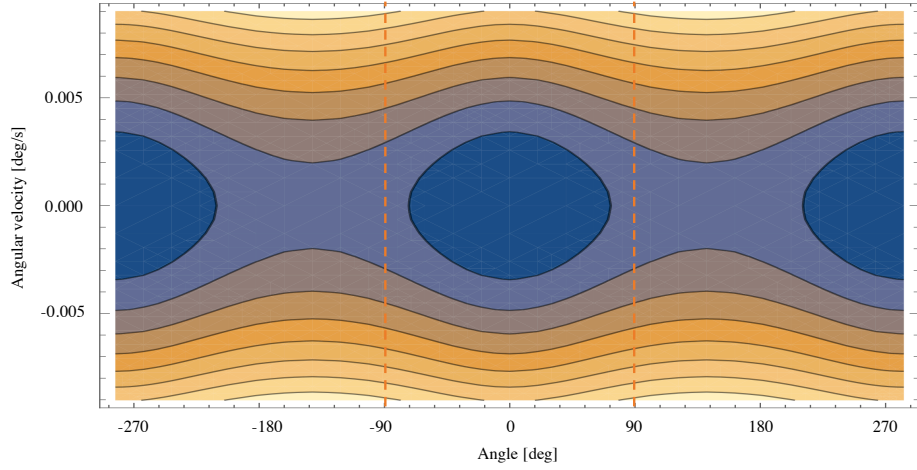
Figure 10. Lyapunov function

in those subsets $\dddot{V}(\boldsymbol{\theta}_x \in Z_1)$ and $\dddot{V}(\boldsymbol{\theta}_x \in Z_2)$, the function goes to zero. This means the Lyapunov candidate meets the asymptotic stability condition of M&C theorem. The third derivative Lyapunov function is given as
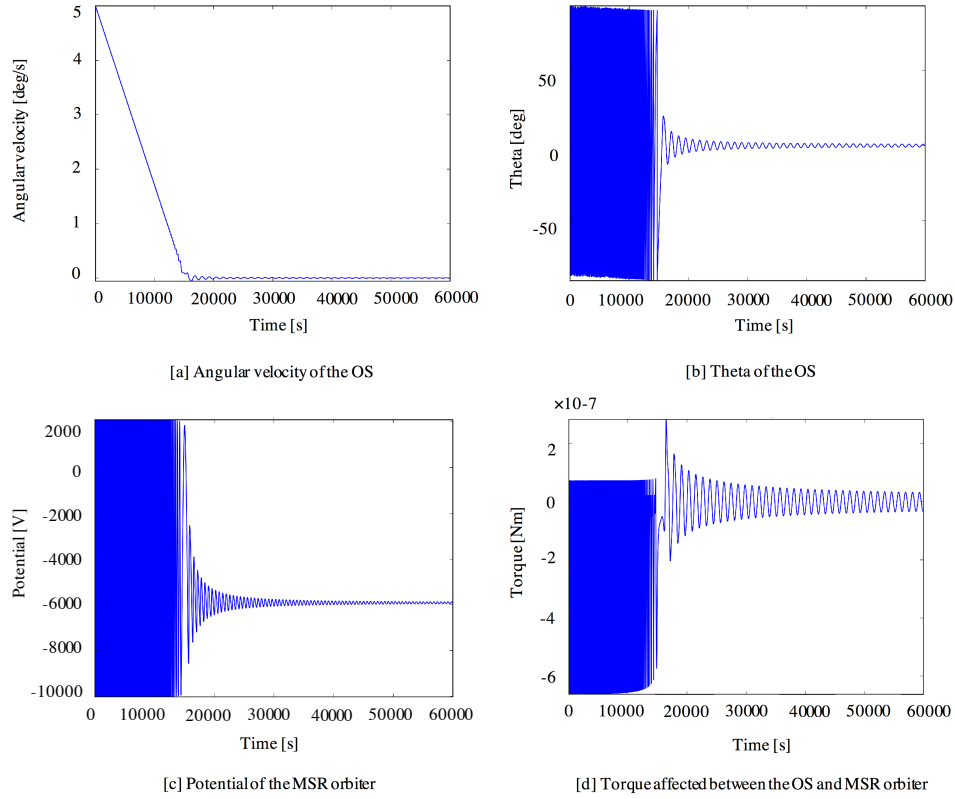
$$\dddot{V}(\boldsymbol{\theta} \in Z_1) = -\frac{16\gamma\phi_{max}}{\pi}\left\{\dot{\theta}_x^3 \tan^{-1}(\alpha\dot{\theta}_x)\right\} \tag{39}$$

$$\dddot{V}(\boldsymbol{\theta} \in Z_2) = -\frac{4\alpha\gamma^3\phi_{max}}{\pi J_{xx}^2}\left\{\frac{\sin^4(2\theta_x)}{(1+\sin^2(\theta_x))^2}\right\} \tag{40}$$

The third derivative Lyapunov function $\dddot{V}$ is locally negative definite, hence it can be said that the controller can make the system to be asymptotically stable. This designed controller is used for aligning the attitude of the OS and the performance is shown in next section.

RESULTS

The initial angular velocity ω_0 and attitude θ_0 are set as 5 deg/s and 10 deg. The gain for the controller α is 10000. The controller can converge the attitude into the range of ± 5 deg in 19550 s, which is approximately 5.4 hr in Fig.11 [a]. As seen in Fig.11 [b], the angular velocity is also converged in the range of ± 0.02 deg/s in the same time. Although the attitude can not be completely converged in zero, the pinning force might catch the OS because the pinning force works with any attitude of the OS if the magnetic flux can be intruded into the SC on the orbiter. The error of the attitude ± 5 deg is not huge error, therefore the force is enough to catch the OS in space. In this simulation, the potential of the OS is maintained as positive using the ion gun on the orbiter. To direct the bottom of the OS to the SC on the orbiter, the negative potential of the orbiter is desirable when the potential of the OS is charged up as positive. This controller is working to direct the bottom of the OS to the orbiter because the potential of the orbiter converges to negative value as seen in Fig.11 [c]. The potential of the orbiter does not require to use the maximum positive potential as Tab.2. As this controller works, required maximum potentials are -10 kV as negative and 2.1 kV as positive respectively. Then the required power can be rewritten as 51.0 W when the potential of the orbiter is same value and sign with the potential of the OS as positive. Although the coulomb torque affects between the orbiter and the OS is small in Fig.11 [d], the retrieval system can control the attitude of the OS sufficiently. According to the Mars 2020 mission report, the

16

[a] Angular velocity of the OS

[b] Theta of the OS

[c] Potential of the MSR orbiter

[d] Torque affected between the OS and MSR orbiter

Figure 11. Numerical calculation results of the controller

orbiter has big solar array panels (SAP) which the area is $15 \mathrm{~m}^2$. In this paper, the orbiter has been approximated as one sphere in the sense of the MSM. If the SAP can be designed using a material which can allow charging up, then the convergence time might be shorter than this results because the coulomb torque working on the OS increases.

The relationship between the convergence time t_c and the required maximum power P_r is shown as Fig.12. The required power for the positive potential of the orbiter is smaller than the negative potential because the retrieval system does not require positive potential operation so much if the potential of the OS is maintained as positive. Therefore the maximum required power P_r is the power when the potential of the OS is opposite sign of the potential of the orbiter. The relationship between the power and the time to converge the attitude in the range of ± 5.0 deg is shown as Fig.12. The relationship has strong nonlinearity. Regression analysis express the relationship between the maximum required power and the convergence time as Regression analysis solves the relationship as

$$P_r = 111.10 + \frac{588.73}{\sinh(t_c)} - 30.0\log(t_c). \tag{41}$$

If the orbiter can be charged up with high potential, the convergence time becomes shorter. This regression expression is useful to estimate the convergence time with the power which the orbiter can use. The expression matches those point with the coefficient of determination $R^2 = 0.999$.

17
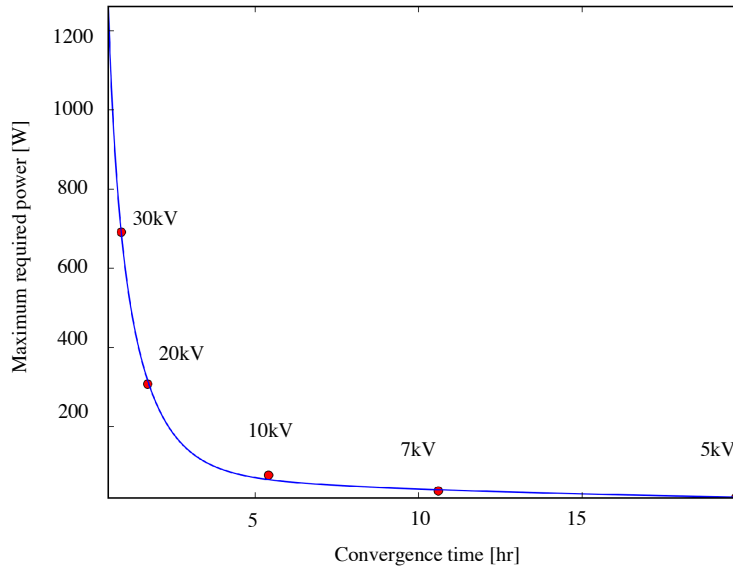
Figure 12. The relationship between the minimum required power and the convergence time

CONCLUSION

Although the proposed OS retriever might be used for other planet's sample return mission, this paper focused on a Martian sample return mission. The possibility of the hybrid sample container retriever was discussed in this paper. The sample container can not be launched to high altitude orbit because a small rockets should be used, hence there are some limitation to operate the proposed system to get the OS automatically in space and those were shown. The effective Debye length becomes small because of the plasma characteristics. The purpose of this system, however, is to fetch the OS automatically, hence few meter of the Debye length is enough to control the state although the orbiter must approach the OS in this range of the effective Debye length. In addition, high power is required to control the potential of the OS and orbiter as well to control the attitude and angular velocity of the OS because the operation is conducted on low altitude orbit. Maximum potential that the orbiter can use is severely limited because of the required power. The designed nonlinear controller can make the attitude and angular velocity of the OS to be converged under those limited condition. The time takes 5.4 hr to ready for getting the OS safely and automatically. The angular velocity and attitude are converged in the range of ± 0.02 deg/s and ± 5.0 deg respectively in the time It is enough to catch the OS using the flux pinning effect. To direct the surface having permanent magnets to the orbiter, however, maximum positive potential is not needed for the orbiter if the potential of the OS is always positive. Then the maximum required power could be rewritten as 51.0 W. The relationship between expected convergence time and the maximum required power was shown. The attitude and angular velocity can be rapidly controlled using the designed controller if the orbiter can use bigger power for this operation. MSM model was used calculating the electrostatic interaction between the OS and the orbiter, however the orbiter is approximated as one sphere in this paper. The orbiter has big SAP in the Mars 2020 mission, therefore the convergence time might be shorter if the SAP consists of a material that allows charging up well. Those effect must be investigated to improve the time for the proposed retrieval system.

18

REFERENCES

[1] Firouz Naderi, Christian Cazaux, and et.al. The nasa/cnes mars sample return - a status report. *Acta Astronaut.*, Vol. 54, No. 8, pp. 601–617, 2004.

[2] Benton C. Clark. Mars sample return: The critical next step. *Acta Astronaut.*, Vol. 61, No. 1-6, pp. 95–100, 2007.

[3] Richard L. Mattingly. The many faces of the mars sample return mission architecture. *27th Annual AAS Guidance and Control Conference,*, AAS 05-066, Breckenridge, Colorado, February 2005.

[4] Brent Sherwood. Mars sample return: Architecture and mission design. *Acta Astronaut.*, Vol. 53, pp. 353–364, 2003.

[5] William O'Neil and Christian Cazaux. The mars sample return project. *Acta Astronaut.*, Vol. 47, pp. 453–465, 2000.

[6] Phil Christensen and Lisa May. Mission concept study: Planetary science decadal survey msr orbiter mission. Technical report, National Aeronautics and Space Administration, 2010.

[7] Phil Christensen and Lisa May. Mission concept study: Planetary science decadal survey msr lander mission. Technical report, National Aeronautics and Space Administration, 2010.

[8] John Dankanich and Eric Klein. Mars ascent vehicle development status. *IEEE Aerospace Conference*, Big Sky, USA, March 2012.

[9] R Mitheltree, R Braun, and et.al. Earth entry vehicle for mars sample return. *51th Internatinal Astronautics Federation Congress*, IAF-00-Q.3.04, Rio de Janeiro, Brazil, Octorber 2000.

[10] Robert Dillman, Bernard Laub, and et.al. Development and test plans for the msr eev. *2nd International Planetary Probe Workshop*, Moffett Field, USA, April 2005.

[11] Scott Perino and Javid Bayandor. A rapid analysis methodology for earth entry vehicle development. *29th Congress of the Internatinal Council of the Aeronautical Science*, Petersburg, Russia, September 2014.

[12] R Carta, D Filippetto, and et.al. Sample canister capture mechanism for mars sample return: Functional and environmental test of the elegant breaddoard model. *Acta Astronaut.*, Vol. 117, pp. 99–115, 2015.

[13] Richard Kornfeld, Joe Parrish, and et.al. Mars sample return: Testing the last meter of rendezvous and sample capture. *J. Spacecr. Rockets*, Vol. 44, No. 3, 2007.

[14] Frances Zhu, Laura Jones-Wilson, and et.al. Capturing and docking spacecraft with flux pinned interfaces. *International Astronautical Congress*, IAC-16-C1.9.4, Guadalajara, Maxico, September 2016.

[15] S Clerc, H Renault, and et.al. Control of a magnetic capture device for autonomous in-orbit rendezvous. *The International Federation of Automatic Control*, Vol. 44, pp. 2084–2089, Milano, Italy, August-September 2011.

[16] Massimo Vetrisano, Nicolas Thiry, and et.al. Detumbling large space debris via laser ablation. *IEEE Aerospace Conference*, Big Sky, USA, March 2015.

[17] Rubbel Kumar and Raymond Sedwick. Despinning orbital debris before docking using laser ablation. *J. Spacecr. Rockets*, Vol. 52, No. 4, pp. 1129–1134, 2015.

[18] Massimo Vetrisano, Camilla Colombo, and et.al. Asteroid rotation and orbit control via laser ablation. *Adv. Space Res.*, Vol. 57, No. 8, pp. 1762–1782, 2016.

[19] Daan Stevenson and Hanspeter Schaub. Multi-sphere method for modeling spacecraft electrostatic forces and torques. *Adv. Space Res.*, Vol. 51, pp. 10–20, 2013.

[20] Hanspeter Schaub and Daan Stevenson. Prospects of relative attitude control using coulomb actuation. *J. of Astronaut. Sci.*, Vol. 60, pp. 258–277, 2013.

[21] Trevor Bennett and Hanspeter Schaub. Touchless electrostatic three-dimensional detumbling of large axi-symmetric debris. *J. of Astronaut. Sci.*, Vol. 62, pp. 233–253, 2015.

[22] Daan Stevenson and Hanspeter Schaub. Electrostatic spacecraft rate and attitude control- experimental results and performance considerations. *Acta Astronaut.*, Vol. 119, pp. 22–33, 2016.

[23] Daan Stevenson and Hanspeter Schaub. Terrestrial testbed for remote coulomb spacecraft rotation control. *Intl. J. Space Sci. Eng.*, Vol. 2, pp. 96–112, 2014.

[24] Trevor Bennett, Daan Stevenson, and et.al. Prospects and challenges of touchless electrostatic detumbling of small bodies. *Adv. Space Res.*, Vol. 56, pp. 557–568, 2015.

[25] Laura Jones, William Wilson, and et.al. Desgin parameters and validation for a non-contacting flux-pinned docking interface. *AIAA Space 2010 Conference and Exposition*, Anaheim, USA, August-September 2010.

[26] Carl Seubert, Laura Stiles, and et.al. Effective coulomb force modeling for spacecraft in earth orbit plasmas. *Adv. Space Res.*, Vol. 54, pp. 209–220, 2014.

[27] Dwight Nicholson. *Introduction to Plasma Theory*. Krieger, Melbourne, USA, 1992.

[28] Erik Hogan and Hanspeter Schaub. Linear stability and shape analysis of spinning three-craft coulomb formations. *Celest. Mech. Dyn. Astron.*, Vol. 112, pp. 131–148, 2012.

[29] Lyon King, Gordon Parker, and et.al. Study of interspacecraft coulomb forces and implications for formation flying. *J. Propul. Power*, Vol. 19, pp. 497–505, 2003.

[30] Shuquan Wang and Hanspeter Schaub. Nonlinear charge control for a collinear fixed shape three-craft equilibrium. *AIAA Guidance, Navigation and Control Conference*, Toronto, Canada, August 2010.

[31] Ravi Inampudi and Hanspeter Schaub. Orbit radial dynamic analysis of two-craft coulomb formation at libration points. *J. Guid. Control Dyn.*, Vol. 37, pp. 682–691, 2014.

[32] Drew Jones and Hanspeter Schaub. Collinear three-craft coulomb formation stability analysis and control. *J. Guid. Control Dyn.*, Vol. 37, pp. 224–232, 2014.

[33] D Gurnett and A Bhattacharjee. *Introduction to Plasma Physics: With Space and Laboratory Applications*. Cambridge University Press, Cambridge, United Kingdom, 2005.

[34] Hanspeter Schaub and Zolta'n Sternovsky. Active space debris charging for contactless electrostatic disposal maneuvers. *Adv. Space Res.*, Vol. 53, pp. 110–118, 2014.

[35] Erik Hogan. Impact of tug and debris sizes on electrostatic tractor charging performance. *Adv. Space Res.*, Vol. 55, pp. 630–638, 2015.

[36] Carl Seubert and Hanspeter Schaub. Rotational stiffness study of two-element tethered coulomb structures. *J. Spacecr. Rockets*, Vol. 48, pp. 488–497, 2011.

[37] Carl Seubert, Stephen Panosian, and et.al. Attitude and power analysis of two-node multitethered coulomb strictire. *J. Spacecr. Rockets*, Vol. 48, pp. 1033–1045, 2011.

[38] I. H. Hutchinson. *Principles of Plasma Diagnostics*. Cambridge University Press, Cambridge, United Kingdom, 2002.

[39] N. Murdoch, D. Izzo, and et.al. Electrostatic tractor for near earth object deflection. *59th International Astronautical Congress*, IAC-08-A3.I.5, Glasgow, Scotland, September- October 2008.

[40] Marissa Vogt, Paul Withers, and et.al. Maven observations of dayside peak electron densities in the ionosphere of mars. *J. Geophys. Res.*, Vol. 122, pp. 891–906, 2017.

[41] M. Benna, P Mahaffy, and et.al. First measurements of composition and dynamics of the martian ionosphere by maven's neutral gas and ion mass spectrometer. *Geophys. Res. Lett.*, Vol. 42, pp. 8958–8965, 2015.

[42] W Hanson, S Sanatani, and et.al. The martian ionosphere as observed by the viking retarding potential analyzers. *J. Geophys. Res.*, Vol. 82, pp. 4351–4363, 1977.

[43] Rejean Grard. Solar photon interaction with the martian surface and related electrical and chemical phenomena. *Icarus*, Vol. 114, pp. 130–138, 1995.

[44] R Ergun, M Morooka, and et.al. Dayside electron temperature and density profiles at mars first results from the maven langmuir probe and waves instrument. *Geophys. Res. Lett.*, Vol. 42, pp. 8846–8853, 2015.

[45] C Fowler, L Andersson, and et.al. The first situ electron temperature and density measurements of the martian nightside ionosphere. *Geophys. Res. Lett.*, Vol. 42, pp. 8854–8861, 2015.

[46] Jpseph E. Borovsky Robert F. Pfaff and David T. Young. *Measurement Techniques in Space Plasmas:Particles*. American Geophysical Union, Washington, D.C., USA, 1998.

[47] Erik Hogan and Hanspeter Schaub. Impacts of hot space plasma and ion beam emission on electronstatic tractor performance. *IEEE Transactions on Plasma Science*, Vol. 43, pp. 3115–3129, September 2015.

[48] M. Schmidt R. Hippler, S. Pfau and K. H. Schoenbach. *Low Temperature Plasma Physics: Fundamental Aspects and Applications*. Wiley, Berlin, Germany, 2001.

[49] B Draine and E Salpeter. On the physics of dust grains in hot gas. *Astrophys. J.*, Vol. 231, pp. 77–94, 1979.

[50] Alexander Kordyuk. Magnetic levitation for hard superconductors. *J. Appl. Phys.*, Vol. 83, pp. 610–612, 1997.

[51] Laura Jones and Mason Peck. Control strategies utilizing the physics of flux-pinned interfaces for spacecraft. *AIAA Guidance, Navigation and Control Conferenceation and Control Conference*, Oregon, USA, August 2011.

[52] T Shibata and S Sakai. Design method for the micro vibration isolator using flux pinning effect for satellites. *AIAA Astrodynamics Specialist Conference*, Long beach, USA, September 2016.